An X-ray Absorption Study of Two $VOCl_3$-Modified Silicas: Evidence for Chloride−Silica Interactions

Eric W. Deguns,[†] Ziyad Taha,[‡] George D. Meitzner,[§] and Susannah L. Scott*[,†,‡]

Departments of Chemistry and Chemical Engineering, University of California, Santa Barbara, California 93106-5080, and Materials Research & Technology Institute, University of Texas, El Paso, Texas 79968-0685

Received: September 11, 2004; In Final Form: December 25, 2004

The structures of the sites formed in the gas−solid reactions of $VOCl_3$ with the surfaces of a fumed silica (Aerosil) and a silica gel (Sylopol) were investigated by using X-ray absorption spectroscopy. XANES and EXAFS analysis at the vanadium K-edge reveal that the sites have a uniform first coordination sphere regardless of the origin or the extent of hydroxylation of the silica support (controlled by thermal treatment in vacuo at 100 and 500 °C). Analysis of the second coordination sphere was limited by the lack of structural uniformity. EXAFS curve-fitting confirmed that the sites are $\equiv SiOVOCl_2$, but revealed an unexpected asymmetry in the V−Cl bond distances. The latter is suggested to be a manifestation of silicon−chloride interactions.

Introduction

Supported vanadium catalysts effect the partial oxidation of hydrocarbons,[1] as well as the partial reduction of NO_x.[2] Catalytic activity requires the dispersion of vanadium on an oxide surface, such as that of silica or alumina.[3−5] Much effort has been invested in understanding the structures of the active sites and the nature of the metal−support interactions.[6−9] These studies are usually complicated by the presence of multiple vanadium sites. Even in the relatively simple V/SiO_2 system, which at low loadings is believed to contain only $(\equiv SiO)_3V{=}O$ sites,[5,10] complexity in the vibrational spectrum has called into question some assignments thought to be well-established.[11]

The use of volatile metal complexes to modify oxide surfaces may result in better dispersion of the active sites than conventional wetness impregnation or sol−gel methods. Thus, the gas−solid reaction of $VOCl_3$ with silica has been reported to generate isolated vanadium sites, although these were described as a mixture of $\equiv SiOVOCl_2$, $(\equiv SiO)_2VOCl$, and $(\equiv SiO)_3VO$, distributed depending on the thermal pretreatment (and hence degree of hydroxylation) of the silica surface.[12,13] The formation of multiple sites is consistent with a model for the surface of amorphous silica with randomly distributed hydroxyl groups. Nevertheless, we found that grafting $VOCl_3$ at ambient temperature onto the surface of an Aerosil silica yields a material whose vanadium sites are both isolated and uniform, regardless of the extent of surface hydroxylation (controlled by heating, from 25 to 500 °C).[14,15] From the amount of chemisorbed V and the yield of HCl, we inferred that each accessible surface hydroxyl reacts according to eq 1:

$$\equiv SiOH + VOCl_3 \rightarrow SiOVOCl_2 + HCl \qquad (1)$$

The formation of uniform grafted sites under these reaction conditions was confirmed by ^{51}V MAS NMR. The spectrum of $VOCl_3$ chemisorbed at room temperature onto silica consists of a single isotropic resonance, at −293 ppm.[14] This chemical shift, assigned to $\equiv SiOVOCl_2$, agrees well with those of analogous molecular complexes $VOCl_2(O^iPr)$ (−307 ppm)[16] and $[VOCl_2(OCH_2CH_2OPh)]$ (−281 ppm),[17] and excludes the presence of physisorbed $VOCl_3$ (0 ppm), $(\equiv SiO)_2VOCl$ (−540 ppm),[18] and $(\equiv SiO)_3VO$ (−676 to −736 ppm).[19,20] A detailed investigation of the magnetic shielding interactions and quadrupole interaction parameters of $VOCl_3$-modified silica confirmed that the grafted vanadium exists in a distorted tetrahedral environment.[21]

Although the techniques used thus far to investigate silica-supported $VOCl_3$ have defined the first coordination sphere of the grafted vanadium, they have shed little light on the metal−support interaction. In view of the interest in well-defined heterogeneous catalysts, we applied X-ray absorption spectroscopy (XAS) to the structural characterization of grafted $VOCl_3$ and the nature of its silica interactions.

Experimental Section

Sample Preparation. The amorphous silicas used in this study are Aerosil-200 (a fumed silica from Degussa) and Sylopol 952X-1836 (a silica gel from Grace-Davison). The Aerosil silica (referred to hereafter as A200) has a surface area of (183 ± 1) m^2/g, a primary particle size of 12 nm, and no significant microporosity. The Sylopol silica (referred to hereafter as S952X), with a surface area of (249 ± 2) m^2/g, is composed of particles of average size 33 μm, with a pore volume of 1.61 mL/g. Thermal pretreatment of each silica sample is indicated by its appended number. For example, A200-100 denotes a sample of Aerosil-200 treated at 100 °C. To ensure reproducibility, each sample was heated under dynamic vacuum ($<10^{-4}$ Torr) at the designated temperature for a minimum of 4 h.

$VOCl_3$ (99.999+%, Aldrich) was stored under vacuum in a glass bulb equipped with a Teflon stopcock. Excess $VOCl_3$ was transferred onto the silica as the vapor, via an all-glass high vacuum line equipped with ground glass stopcocks. $VOCl_3$ reacts slowly with hydrocarbon-based vacuum greases. Although this does not appear to affect the preparation of vanadium-

* To whom correspondence should be addressed. Fax: 1-805-893-4731. E-mail: sscott@engineering.ucsb.edu.
[†] Department of Chemistry, University of California.
[‡] Department of Chemical Engineering, University of California.
[§] University of Texas.

10.1021/jp045886y CCC: $30.25
Published on Web 03/01/2005

modified silicas, the grease was replaced frequently. Alternately, the joints and stopcocks were greased with perfluorinated Krytox, which is inert toward $VOCl_3$. After desorption of unreacted $VOCl_3$ to a liquid N_2 trap, the vanadium-modified silica was obtained as a white powder. Exposure of the sample to even traces of moisture during or after grafting was readily detected, since it resulted in an immediate color change to yellow.

Vanadium analysis was performed in air at the end of each experiment. Each sample was weighed and stirred in 1.0 M H_2SO_4 to which 3.5% aqueous H_2O_2 (0.03 mL/mL sample solution) was added to extract the vanadium as its peroxo complex. The solution was filtered before recording its UV−vis spectrum in a 1 cm quartz cuvette, referenced to a H_2SO_4/H_2O_2 solution containing approximately the same concentration of H_2O_2. Spectra were recorded on a Varian Cary 1E spectrophotometer. The orange peroxovanadium complex has a distinct peak in the visible at $\lambda_{max} = 453$ nm ($\epsilon = 632$ M^{-1} cm^{-1}). A calibration curve was prepared with standard solutions of ammonium metavanadate.

On A200 pretreated at 100 °C, the V loading was (2.98 ± 0.11) wt %, corresponding to (0.58 ± 0.02) mmol V/g silica. When A200 was pretreated at 500 °C, causing partial dehydroxylation of the silica surface, the V loading was (2.23 ± 0.13) wt %, or (0.44 ± 0.03) mmol V/g silica. Loadings on S952X were higher for the same pretreatment temperature, reflecting both its higher surface area and hydroxyl content. After pretreatment at 100 °C, the V loading was (5.84 ± 0.18) wt %, or (1.15 ± 0.04) mmol V/g silica. After pretreatment at 500 °C, the V loading was (4.14 ± 0.5) wt %, or (0.82 ± 0.01) mmol V/g silica. Each reported metal loading is the average measurement for at least 4 independently prepared samples.

XAS Spectrum Acquisition. Experiments were performed at the Stanford Synchrotron Radiation Laboratory (SSRL) on beamline BL2-3 (Bend), operated at 3.0 GeV with a current of 75−100 mA. X-rays were monochromatized via reflection from Si(111) crystals through a 1 mm entrance slit. The incident beam was detuned 40−50% to suppress harmonics. Samples were mounted at 45° to the beam, to collect transmission and fluorescence spectra simultaneously. The intensity of the incident beam was measured with a He-filled ion chamber detector. Transmitted X-rays were detected in a N_2-filled ion chamber, then passed through a vanadium calibration foil into a third, N_2-filled ion chamber. Fluorescence from the sample was recorded with an Ar-purged Lytle detector without Soller slits.

Sample powders were held in aluminum plates with 35 × 5 × 2 mm^3 slots, between windows of 6.0 μm polypropylene film (Chemplex no. 425) affixed with double-sided tape to each side of the plate. Loading of the sample holders was performed under N_2 in a glovebox, to prevent sample hydrolysis. Samples instantly changed color from white to yellow, and eventually to green, when exposed to atmospheric moisture. Spectroscopic analysis of imperfectly sealed samples was thus readily avoided. Spectra were recorded at room temperature, except where noted. Low-temperature spectra were recorded in an Oxford Instruments liquid He flow cryostat, in transmission mode, using aluminum sample plates with 10 × 4 × 2 mm^3 window slots. Three sweeps were acquired for each sample (total acquisition time ~1 h). The unprocessed spectra were then averaged to improve the signal-to-noise ratio.

Data Analysis. XANES and EXAFS spectra were analyzed with WinXAS (v. 3.1).[22] Energy calibration was performed by using the spectrum of the V calibration foil (K-edge 5465.0 eV),[23] recorded simultaneously for each sample. Spectra were background corrected by subtracting a linear fit to the preedge region extrapolated the length of the entire spectrum, and then normalized by a 7th degree polynomial fitted to the postedge region. Each XANES region was extracted from a complete XAS spectrum to include data up to 150 eV after the K-edge. Preedge peak heights and positions were computed via a least-squares fit of the XANES region with a Lorentzian function for the normalized K-edge and an arctan function for the pre-peaks.

EXAFS spectra were k^3-weighted and fitted by a polynomial spline with 6 knots between 1.0 and 16.1 $Å^{-1}$. Subtraction of this spline decreases contributions from low-frequency atomic X-ray absorption fine structure (AXAFS).[24] A Hanning window was applied to the first and last 10% of the data range before Fourier transformation to *R*-space. The *k*-space spectra were fitted to single-scattering paths with use of the EXAFS equation, eq 2, with least-squares refinement.[25]

$$\chi(k) = \sum_i \frac{N_i S_i(k) F_{i(k)}}{kR_i^2} \exp(2k^2\sigma^2) \exp\left(\frac{-2R_i}{\lambda}\right) \sin(2kR_i + \phi_i(k)) \quad (2)$$

For each shell, N is the number of scatterers in the ith shell at a distance R from the absorber. The Debye−Waller factor, σ^2, is the root-mean-squared relative displacement of the scatterer, λ is the mean-free path of the photoelectron, and $\phi(k)$ is its phase shift. Phase shift and backscattering amplitude functions were calculated with FEFF 8.2.[26,27] Starting distances for curve fits were obtained from crystal structure parameters of model compounds.

The residual $\mathscr{R}$ is defined by eq 3, where $\chi_{obs}(k_i)$ is the experimental data and $\chi_{calc}(k_i)$ is the calculated EXAFS.

$$\mathscr{R} = \frac{\sum_{i=1}^{N} |\chi_{obs}(k_i) - \chi_{calc}(k_i)|}{\sum_{i=1}^{N} |\chi_{obs}(k_i)|} \cdot 100\% \quad (3)$$

$\mathscr{R}$ cannot be used to assess improvement in the fit relative to an increase in the number of variable parameters. Instead, a χ^2-like statistic such as ϵ^2 can be used to normalize the deviation at each data point, using the variance at that point (σ_i^2), and to introduce a penalty for an increased number of degrees of freedom ν, eq 4.[28]

$$\epsilon^2 = \frac{(N_{idp}/\nu) \sum_{i-1}^{N} k^6 (\chi_{obs}(k_i) - \chi_{calc}(k_i))^2/\sigma_i^2}{N} \quad (4)$$

N represents the number of data points being fitted while ν is the difference between the number of independent data points, N_{idp}, and the number of variable parameters, N_{var}. N_{idp} is calculated with eq 5:

$$N_{idp} = \frac{2\Delta k \Delta R}{\pi} + b \quad (5)$$

where Δk is the energy range of useful EXAFS (in *k*-space) and ΔR is the region of meaningful data in the Fourier transformed spectrum.[29] The most restrictive case requires the value $b = 0$, but values of 1 or 2 have also been proposed.[30,31]

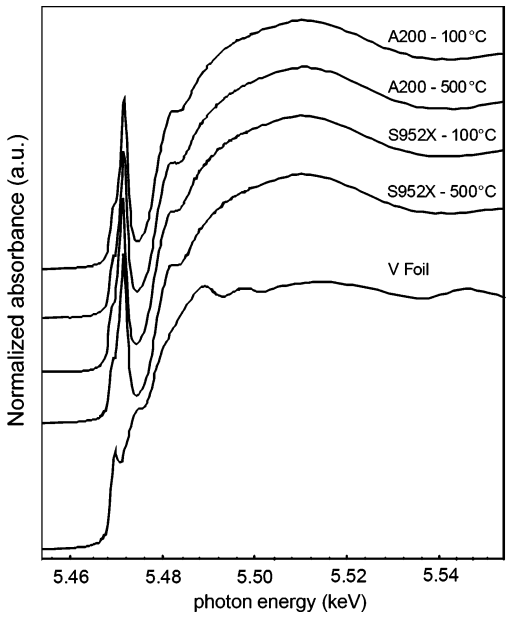

Figure 1. Comparison of vanadium K-edge XANES regions for V metal calibration foil and $VOCl_3$-modified silicas.

In practice, calculating ϵ^2 is difficult and potentially unreliable, since the variance at each data point introduces both statistical and nonstatistical errors into the fit. Instead, we used an *F*-test to evaluate the improvement in the fit, eq 6.[32−34]

$$F = [(\varepsilon_2{}^2 - \varepsilon_1{}^2)/2]/[\varepsilon_2{}^2/\nu] \quad (6)$$

The value of ε for a given fit is calculated with eq 7.

$$\varepsilon = \sqrt{\sum_{i=1}^{N} \frac{k^6(\chi_{obs}(k_i) - \chi_{calc}(k_i))^2}{N}} \quad (7)$$

Results and Discussion

XANES Analysis. Normalized V K-edge XANES spectra of $VOCl_3$-modified A200-100, A200-500, S952X-100, and S952X-500, as well the vanadium metal calibration foil, are shown in Figure 1. Energy scales were calibrated at the first inflection point (K-edge) in the foil calibration spectrum (5465.0 eV). The K-edges of the $VOCl_3$/silica samples are shifted by ca. 18 eV to higher energy relative to the foil, within the range of K-edge energies reported for known V(V) compounds.[35] The XANES regions for all four samples are indistinguishable, indicating that their electronic structures and site symmetries are the same.

The number and positions of the preedge features are most easily discerned in a first derivative representation of the XANES region, Figure 2. There is a prominent preedge peak (B) with a low-energy shoulder (A) in the XANES region. These features arise from K-edge dipolar transitions to the (largely nonbonding) 3d orbitals. The displacement of the most intense preedge peak from the energy of the foil K-edge, 4.9 eV, is consistent with preedge positions in other four- and five-coordinate V(V) materials, Table 1.[35,36] A shoulder on the main absorption edge (C) appears at ca. 13 eV from the foil K-edge. This feature may be a 1s → 4p shakedown transition.[37] The direct 1s → 4p transition, expected at ca. 22 eV from the foil K-edge,[35,36] is likely masked by the main absorption edge.

Spectral Changes upon Hydrolysis. Dramatic changes in the XANES region were noted when the $VOCl_3$/silica samples were exposed to air. When a sample of vanadium-modified S952X-100 was exposed to air for 20 min, its color changed from white to yellow. After air exposure for 2 days, the completely hydrolyzed sample was green. The evolution of the XANES region during sample decomposition is shown in Figure 3. The normalized intensity of the preedge peak (B, Figure 2) decreases, from 0.67 in the intact sample to 0.53 in the

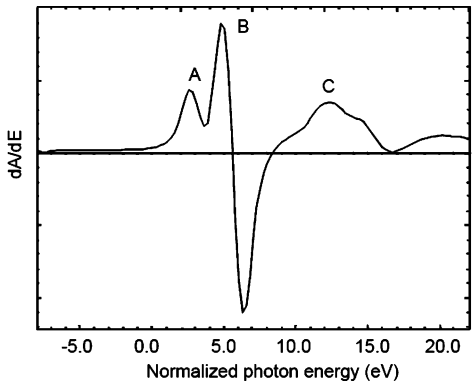

Figure 2. First derivative of the XANES region for $VOCl_3$-modified S952X-500. The energy scale is relative to the V foil K-edge (5645.0 eV).

TABLE 1: Peak Positions[a] in V K-edge XANES

sample	*A*	*B*[b]	*C*	main edge	ref
$VOCl_3$/A200-100	2.3	4.8 (0.66)	13.2	18.4[c]	this work
$VOCl_3$/A200-500	2.4	4.9 (0.67)	13.1	18.3[c]	this work
$VOCl_3$/S952X-100	2.4	4.9 (0.67)	12.8	18.2[c]	this work
$VOCl_3$/S952X-500	2.3	4.9(0.69)	12.9	18.4[c]	this work
$VOCl_3$/S952X-100, decomposed	-	1.9 (0.53)		15.9[c]	this work
V_2O_5	2.6	5.6		15.1	35
	2.9	6.1 (0.62)		16.6	5
		5.6		16.6	38
		4.6 (0.74)			36
NH_4VO_3	3.0	4.8	12.1	17.2	35
	3.3	5.6 (0.89)		18.0	5
		4.8		18.0	38
		3.8 (0.92)			36
V_2O_5/SiO_2, hydrated		6.0 (0.56)		16.7	5
V_2O_5/SiO_2, dehydrated	3.3	6.0 (0.76)		18.9	5

[a] Relative to V foil calibration standard (5465.0 eV). The uncertainty in peak positions is estimated to be ±0.2 eV. [b] Values in parentheses represent the peak intensity, normalized to the step height of the K-edge. [c] Main edge position calculated by Lorentzian least-squares fitting (see the Experimental Section).

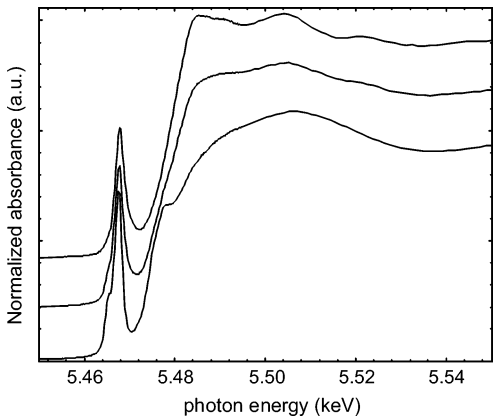

Figure 3. Evolution of V K-edge XANES spectra for vanadium-modified S952X-100 during hydrolysis: (bottom) intact sample; (middle) partially hydrolyzed sample, exposed to air for 20 min; (top) completely hydrolyzed sample, exposed to air for 2 days.

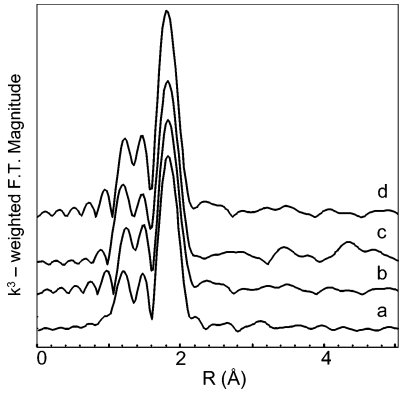

Figure 4. Fourier transformed k^3-weighted EXAFS of $VOCl_3$-modified silicas: (a) S952X-500; (b) S952X-100; (c) A200-500; and (d) A200-100.

SCHEME 1: Model Surface Species Refined to EXAFS Data.

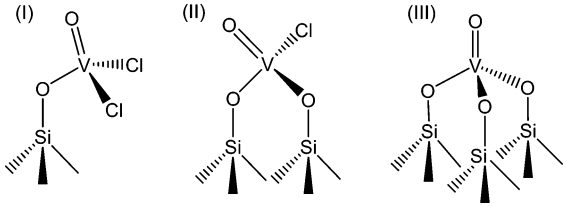

completely hydrolyzed sample, while the shoulder (A, Figure 2) on the preedge peak disappears. The K-edge shoulder (C, Figure 2) becomes less prominent, while a new feature, assigned to the 1s → 4p transition, appears at 21 eV. The spectrum of the fully hydrolyzed sample is similar to that of hydrated V_2O_5/SiO_2.[35,36]

Principal component XANES analysis was used to estimate the extent of hydrolysis in incompletely hydrolyzed samples.[39] The spectrum of the partially decomposed yellow sample described above (air exposed for 20 min) contains 41% of the characteristic features of the fully hydrolyzed sample, while the "intact" sample is less than 2% hydrolyzed. The extent of hydrolysis evident in the spectra of the other "intact" samples (i.e., $VOCl_3$-modified S952X-500, A200-500, and A200-100) is 1%, 4%, and 2.5%, respectively. These values were assumed to be statistically insignificant for the purposes of EXAFS analysis.

EXAFS Analysis of the First Coordination Sphere. The Fourier transformed k^3-weighted EXAFS for each of the $VOCl_3$-modified silicas are compared in Figure 4. The spectra are nearly identical below $R = 2.5$ Å, confirming that all samples have the same first coordination sphere for vanadium. The EXAFS for $VOCl_3$-modified S952X-500 was fitted to single-scattering models containing two oxygen shells (terminal, bridging), one chlorine shell and one silicon shell, Scheme 1. Only model I refined successfully to the EXAFS data. Attempts to refine the data to a monochloro complex, $(\equiv SiO)_2VOCl$ (model II), or a tripodally supported vanadyl site, $(\equiv SiO)_3VO$ (model III), were unsuccessful. Incorporation of a third oxygen shell representing coordinated siloxane ligands, as in $(\equiv SiO)(\equiv Si_2O)_nVOCl_2$, did not lead to an improved fit. Fits to the dinuclear models $[VOCl_2]_2(\mu\text{-}OSi\equiv)_2$ and $[\equiv SiOVOCl]_2(\mu\text{-}Cl)_2$ also failed to converge. Refinement of the single-scattering $\equiv SiOVOCl_2$ model to data for other $VOCl_3$-modified silicas gives identical atomic path fits, within statistical uncertainty (see the Supporting Information). Thus we conclude that model I best describes the first coordination sphere of vanadium in $VOCl_3$-modified silicas.

TABLE 2: EXAFS Fits[a] for Single Scattering Paths in the $\equiv SiOVOCl_2$ Model (equivalent chlorides) Fitted against Data from $VOCl_3$-Modified S952X-500

		spectrum recorded at 295 K[c]			spectrum recorded at 20 K[d]		
path	CN[b]	bond length, Å	σ^2, Å^2	E_0, eV	bond length, Å	σ^2, Å^2	E_0, eV
V═O	1	1.57	0.00036	−7.58	1.58	0.00244	−5.55
V−O	1	1.78	0.00155	−7.58	1.78	0.00014	−5.55
V−Cl	2	2.16	0.01156	−2.52	2.16	0.00951	−3.22
V−Si	1	3.13	0.02753	4.68	3.21	0.01456	3.77

[a] Errors for first-shell scattering fits calculated against EXAFS data, in the absence of systematic fitting uncertainties, are generally to be accepted as follows: bond lengths ±0.02 Å, σ^2 ±20%, E_0 ±20%.[42] [b] Coordination numbers fixed (see text). [c] $S_o^2 = 0.88$, residual = 19.51 for this model optimization. [d] $S_o^2 = 0.91$, residual = 22.03 for this model optimization.

The coordination numbers obtained from the initial fit of the S952X-500 data were very close (±10%) to the integer values expected for uniform $\equiv SiOVOCl_2$ sites (Table 1, Supporting Information), with the exception of the V−Si path (see below). Therefore, to reduce the number of independent variables in the fit, coordination numbers were subsequently fixed at their integer values. For each path, the following free variables were then sequentially refined: path length (R), Debye−Waller factor (σ^2), and inner potential energy (E_0). E_0 was constrained for each type of absorber−scatterer pair, e.g., all V−O paths. The amplitude reduction factor (S_o^2) was calculated as a global variable in the fit refinement. Fit parameters are summarized in Table 2. The fitted V═O and V−O distances, at 1.57 and 1.78 Å, respectively, are consistent with those for $VOCl_3$ and vanadyl silanolates, Table 3. When the chloride paths are constrained to be equivalent, the V−Cl bond lengths emerge at 2.16 Å, with an associated Debye−Waller factor σ^2 of 0.0116 Å^2. The bond distance obtained for the V−Cl path is comparable to known vanadyl chlorides (2.12−2.17 Å), Table 3, yet the Debye−Waller factor is an order of magnitude larger than expected (see below).

Multiple scattering paths were added to the $\equiv SiOVOCl_2$ model in an attempt to gain more information about bond angles. Addition of chlorine−chlorine and vanadyl oxygen−chlorine multiple scattering paths did not enhance the fit. Indeed, the spectra show little intensity at 3.0 and 3.8 Å, where V−O−Cl and V−Cl−Cl multiple scattering paths were observed in the gas-phase electron scattering of $VOCl_3$.[40] Destructive interference may cause multiple scattering contributions to be less apparent in EXAFS spectra.[41]

Second Coordination Sphere Analysis. When the coordination number for the silicon shell was freely refined, we obtained the smaller than expected value of 0.68 (Table S1, Supporting Information). When the coordination number is fixed at 1, the fitted V−Si distance is 3.13 Å, and has a large associated Debye−Waller factor ($\sigma^2 = 0.0275$ Å^2), Table 2. Although the V−Si path is poorly resolved, the fitted distance of 3.13 Å is nevertheless comparable to the V−Si distance of 3.13 Å in $[VOCl(OSi^tBu)_2]_3$. Assuming an Si−O distance of 1.61 Å,[45] the fitted V−Si and V−O distances require a Si−O−V angle of $(136 \pm 30)°$. This value compares well to those for molecular vanadium silanolates: for example, the silsesquioxane dimer $[(c\text{-}C_6H_{11})_7(Si_8O_{12})VO]_2$ has Si−O−V angles of 136.0°, 145.6°, and 146.4°,[48] while a cyclic V(IV) silanolate has Si−O−V angles of 134.0° and 135.6°.[49] Noncyclic silanolates tend to have much larger Si−O−V angles, ca. 153° for $VO(OSiPh_3)_3$,[19,45] possibly due to $d_\pi - p_\pi$ overlap. Such overlap is unlikely for the

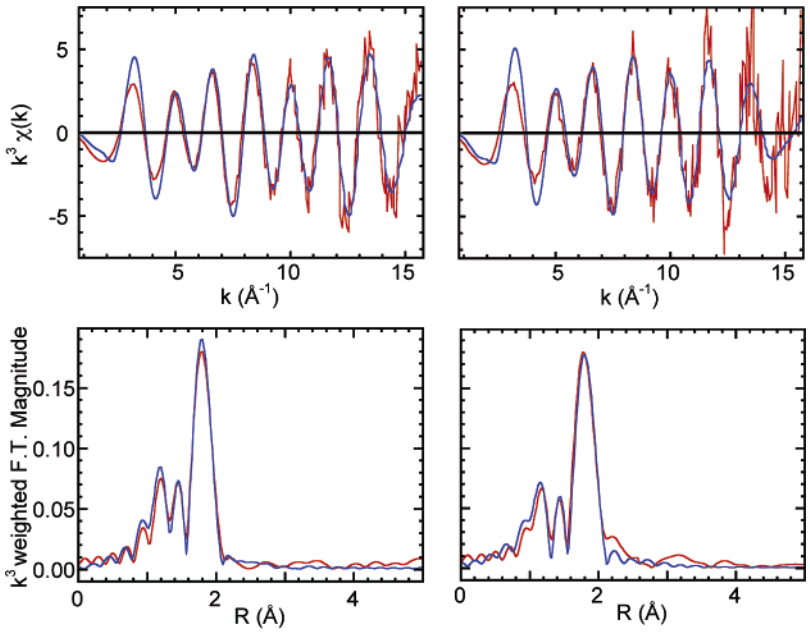

Figure 5. Single-scattering refinement of the ≡SiOVOCl$_2$ model (equivalent chlorides) to EXAFS of (a) $VOCl_3$/S952X-500 at 295 K and (b) at 20 K, in k^3-weighted EXAFS *k*-space (top) and in *R*-space (bottom). Red line: experimental data. Blue line: calculated fit.

TABLE 3: Bond Distances (Å) in Structurally Characterized Vanadyl Chlorides and Silanolates

compound	V=O	V−Cl	V−O	V−Si	method	ref
$VOCl_3$ (solid)	1.562	2.125			XRD	43
		2.124			XRD	44
$VOCl_3$ (gas)	1.570	2.142			electron scattering	40
$VO(OSiPh_3)_3$	1.564		1.743	3.3(4)	XRD	45
			1.745			
			1.739			
$[(c\text{-}C_6H_{11})_7(Si_8O_{12})VO]_2$	1.564		1.772	not reported	XRD	19
			1.737			
			1.746			
$[VOCl(O_2Si^tBu_2)]_3$	1.589	2.1717	1.727	3.13	XRD	46
$VOCl_2(OCH_2CH_2OPh)$	1.5703	2.1570	1.7134		XRD	17
		2.1715				
$VO[OSi(O^tBu)_3]_3$	1.596		1.770	not detected	EXAFS	47

highly electron-withdrawing silica ligand. Furthermore, the EXAFS suggests that the Si−O−V angle in ≡SiOVOCl$_2$ is not linear, since the intensities of multiple scattering paths are significantly enhanced for angles approaching 180°, due to the focusing effect.[50]

We attempted to amplify scattering from the V−Si path using cryogenic cooling to minimize thermal disorder.[51] The *k*-space and *R*-space EXAFS spectra of $VOCl_3$-modified S952X-500, recorded at 295 and 20 K, are compared in Figure 5. Paths associated with the first coordination sphere did not vary beyond their uncertainties from the model refinement to the room temperature data. No additional features were apparent in the data collected at the cryogenic temperature. We conclude that the absence of features in the pseudoradial distribution beyond 2.5 Å for $VOCl_3$/silica materials is a consequence not of thermal motions but of a lack of structural uniformity beyond the first coordination sphere in the ≡SiOVOCl$_2$ sites. Unexpectedly, the Debye−Waller factors did not decrease for the fit to the cryogenic data relative to the room temperature fit. This is likely a consequence of the lower signal-to-noise ratio in the former dataset, which arises because the use of the cryostat requires collection in transmission mode rather than fluorescence and with a smaller beam spot.

Chloride Asymmetry. The ≡SiOVOCl$_2$ model with two equidistant chloride ligands generates a reasonable fit to the experimental data. However, when the V−Cl distances are allowed to vary independently, the fit to the V−Cl paths improves substantially (σ^2 values of 0.00060 and 0.00089 Å^2, compared to 0.0116 Å^2 for the model with equivalent chlorides). The fitted V−Cl distances are 2.10 and 2.22 Å, Table 4. The 0.12 Å asymmetry is much greater than the uncertainty for each path (±0.02 Å).[42,52] The large Debye−Waller factor, 0.0116 Å^2, generated by the fit to the model with equidistant chlorides is likely a consequence of attempting to accommodate both the

TABLE 4: EXAFS Fits[a,b] for Single Scattering Paths of the ≡SiOVOCl$_2$ Model (inequivalent chlorides) to Data Collected for $VOCl_3$/S952X-500 at 295 K, with and without Fourier Filtering[c]

	unfiltered data[d]			filtered data[e]	
path	bond length, Å	σ^2, Å^2	E_0, eV	bond length, Å	σ^2, Å^2
V=O	1.59	0.00231	−0.39	1.59	0.00093
V−O	1.78	0.00074	−0.39	1.78	0.00087
V−Cl	2.10	0.00060	−1.44	2.10	0.00067
V−Cl	2.22	0.00089	−1.44	2.22	0.00104

[a] Errors for first-shell scattering fits calculated against EXAFS data, in the absence of systematic fitting uncertainties, are generally to be accepted as follows: bond lengths ±0.02 Å, σ^2 ±20%, E_0 ±20%.[42] [b] All coordination numbers were fixed at 1 (see text). [c] Back-transformed range for Fourier filtering: R = 0.80−2.2 Å, k = 1.0−16.1 Å^{-1}. The resolution of the data is estimated to be 0.10 Å from $\Delta R = \pi/2\Delta k$, see ref 55. [d] Residual for this curve fit: 15.37. [e] Residual for this curve fit: 16.45.

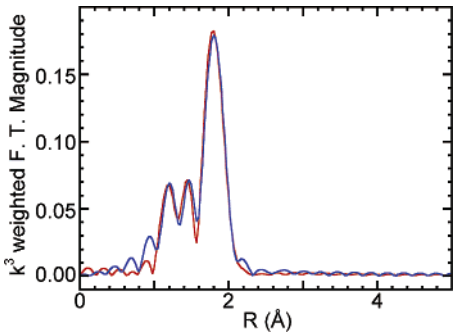

Figure 6. Single-scattering refinement of the ≡SiOVOCl$_2$ model (inequivalent chlorides) to EXAFS of Fourier-filtered VOCl$_3$/S952X-500 at 295 K in k^3-weighted R-space. Red line: experimental data (back-transformed range: $R = 0.80-2.2$ Å, $k = 1.0-16.1$ Å^{-1}). Blue line: calculated fit.

short and long V−Cl paths at their average distance, 2.16 Å, with a large broadening parameter.[53]

The inner potential corrections E_0 are also smaller for both the V−O and V−Cl paths in the inequivalent chloride fit, compared to the equivalent chloride fit. Typically, smaller refined values for E_0 are expected for models which better describe the data.[54] Evidence for chloride asymmetry was found in the EXAFS fits for all of the VOCl$_3$/silica samples (see the Supporting Information).

For the S952X-500 curve fits, the residual decreases from 19.51 to 15.37 when the chloride symmetry is removed, indicating better agreement with the experimental data. However, an increase in fit quality is expected solely as a result of the increased number of variable parameters. Therefore, statistical analysis was performed to assess the improvement in the fit independent of the number of variables. First, spectra were back-Fourier transformed from $R = 0.8$ to 2.3 Å, to isolate contributions from the first-shell scatterers (i.e., VO_2Cl_2). Model refinements were constrained to reduce N_{var} by fixing S_o^2 at 0.96 (an average value obtained in previous fits) and by not refining E_0 (i.e., fixing it at 0). Therefore, the values of N_{var} are 6 and 8 for the equidistant and inequivalent V−Cl fits, respectively. The result of fitting the filtered EXAFS data is shown in Figure 6, with curve fit parameters summarized in Table 4. Bond lengths are identical with those in fits to unfiltered data. The difference between the equivalent and nonequivalent curve fits is best seen overlaid on the filtered k^3-weighted wavevectors, Figure 7.

With $\Delta k = 15.1$ Å^{-1}, $\Delta R = 1.5$ Å, and $b = 0$, the number of degrees of freedom ν is $(14.3 - N_{var})$. The values of ε are therefore 1.18 and 0.64 (see the Experimental Section) for the equivalent and inequivalent chloride fits, respectively. The F-test returns a value of 7.20 for comparison of the fits to the VOCl$_3$/S952X-500 data recorded at 295 K. The critical F value, at the $P = 0.05$ level, for $\nu \approx 6$ is 5.14.[56] Therefore, inclusion of two V−Cl shells is warranted. F-test values of 5.38, 6.46, and 8.24 were obtained for inequivalent chloride fits for VOCl$_3$ grafted onto S952X-100, A200-500, and A200-100, respectively.

Structurally characterized molecular analogues of the surface site ≡SiOVOCl$_2$, i.e., V(O)Cl$_2$(OR) complexes, are rare.[57,58] VOCl$_2$(OCH$_2$CH$_2$OPh) displays a much smaller chloride asymmetry, with V−Cl distances at 2.1570 and 2.1715 Å.[17] The V-(V) center in (V^{V}OCl$_2$)(μ-O)(V^{IV}OCl)(9-fluorenone)$_2$(H$_2$O) also has only slightly asymmetric chloride distances, at 2.1792 and 2.187 Å.[58] The origin of the much greater chloride asymmetry in ≡SiOVOCl$_2$ is proposed to be a consequence of the interaction of one chloride ligand with a silicon atom of the silica surface. Silicon is known to expand its coordination

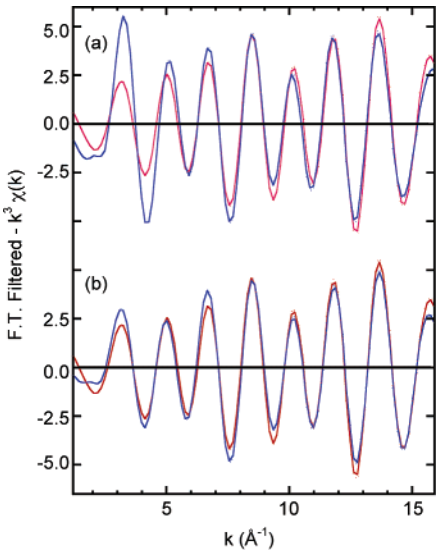

Figure 7. Single-scattering refinement of the ≡SiOVOCl$_2$ models, (a) equivalent chlorides and (b) inequivalent chlorides, to Fourier-filtered EXAFS of S952X-500 in k^3-weighted k-space. Red lines: experimental data (back-transformed range: $R = 0.80-2.2$ Å, $k = 1.0-16.1$ Å^{-1}). Blue lines: calculated fits.

number to five, especially by interaction with halide ions.[59−63] Such an interaction may presage full transfer of chlorine to the silica surface, as was suggested to explain the slow evolution of the IR spectra of grafted SOCl$_2$,[64] TiCl$_4$,[65] and VOCl$_3$.[65] A related transformation of ≡SiOMoCl$_4$ was reported to yield MoOCl$_{3(g)}$ and, presumably, ≡SiCl.[66] The nature of the apparent vanadium−chlorine asymmetry is the subject of an ongoing investigation.

Acknowledgment. Portions of this research were carried out at the Stanford Synchrotron Radiation Laboratory, a national user facility operated by Stanford University on behalf of the U.S. Department of Energy, Office of Basic Energy Sciences.

Supporting Information Available: k^3-weighted k-space and R-space EXAFS spectra and model refinements for VOCl$_3$-modified A200-100 and -500, S952X-100 and -500. This material is available free of charge via the Internet at http://pubs.acs.org.

References and Notes

(1) Ozkan, U. S.; Harris, T. A.; Shilf, B. T. *Catal. Today* **1997**, *33*, 57.
(2) Bosch, H.; Janssen, F. *Catal. Today* **1988**, *2*, 369.
(3) Busca, G.; Centi, G.; Marchetti, L.; Trifiro, L. *Langmuir* **1986**, *2*, 568.
(4) Andersson, A. *J. Solid State Chem.* **1982**, *42*, 263.
(5) Gao, X.; Bare, S. R.; Weckhuysen, B. M.; Wachs, I. E. *J. Phys. Chem. B* **1998**, *102*, 10842.
(6) Centeno, M. A.; Malet, P.; Carrizosa, I.; Odriozola, J. A. *J. Phys. Chem. B* **2000**, *104*, 3310.
(7) Khodakov, A.; Olthof, B.; Bell, A. T.; Iglesia, E. *J. Catal.* **1999**, *181*, 205.
(8) Wachs, I. E.; Weckhuysen, B. M. *Appl. Catal. A* **1997**, *147*, 67.
(9) Inumaru, K.; Misono, M.; Okuhara, T. *Appl. Catal. A* **1997**, *149*, 133.
(10) Takenaka, S.; Tanaka, T.; Yamazaki, T.; Funabiki, T.; Yoshida, S. *J. Phys. Chem. B* **1997**, *101*, 9045.
(11) Magg, N.; Immaraporn, B.; Giorgi, J. B.; Schroeder, T.; Baumer, M.; Dobler, J.; Wu, Z.; Kondratenko, E.; Cherian, M.; Baerns, M.; Stair, P. C.; Sauer, J.; Freund, H.-J. *J. Catal.* **2004**, *226*, 88.
(12) Malygin, A. A.; Volkoa, A. N.; Kol'tsov, S. I.; Aleskovskii, V. B. *Zh. Obshch. Khim.* **1973**, *43*, 1436.
(13) Kol'tsov, S. I.; Malygin, A. A.; Volkoa, A. N.; Aleskovskii, V. B. *Zh. Fiz. Khim.* **1973**, *47*, 988.
(14) Rice, G. L.; Scott, S. L. *Langmuir* **1997**, *12*, 11545.

(15) Rice, G. L.; Scott, S. L. *J. Mol. Catal. A*: *Chem.* **1997**, *125*, 73.
(16) Priebsch, W.; Rehder, D. *Inorg. Chem.* **1985**, *24*, 3058.
(17) Rosenthal, E. C. E.; Girgsdies, F. *Z. Anorg. Allg. Chem.* **2002**, *628*, 1917.
(18) Ghosh, N. N.; Clark, J. C.; Eldridge, G. T.; Barnes, C. E. *Chem. Commun.* **2004**, 856.
(19) Feher, F. J.; Walzer, J. F. *Inorg. Chem.* **1991**, *20*, 1689.
(20) Das, N.; Eckert, H.; Hu, H.; Wachs, I. E.; Walzer, J. F.; Feher, F. J. *J. Phys. Chem.* **1993**, *97*, 8240.
(21) Lapina, O. B.; Mats'ko, M. A.; Mikenas, T. B.; Zakharov, V. A.; Paukshtis, E. A.; Khabibulin, D. F.; Sobolev, A. P. *Kinet. Catal.* **2001**, *42*, 553.
(22) Ressler, T. *J. Synchrotron Radiation* **1998**, *5*, 118.
(23) Bearden, J. A.; Burr, A. F. *Rev. Mod. Phys.* **1967**, *39*, 125.
(24) Wang, W. C.; Chen, Y. *Phys. Status Solidi A* **1998**, *168*, 351.
(25) Sayers, D. E.; Stern, E. A.; Lytle, F. W. *Phys. Rev. Lett.* **1971**, *27*, 1204.
(26) Ankudinov, A. L.; Ravel, B.; Rehr, J. J.; Conradson, S. D. *Phys. Rev. B* **1998**, *58*, 7565.
(27) Ankudinov, A. L.; Bouldin, C.; Rehr, J. J.; Sims, J.; Hung, H. *Phys. Rev. B* **2002**, *65*, 104107.
(28) Bunker, G.; Hasnain, S.; Sayers, D. In *X-ray Absorption Fine Structure*; Hasnain, S. S., Ed.; Ellis Horwood: New York, 1991; p 751.
(29) Lee, P. A.; Citrin, P. H.; Eisenberger, P.; Kincaid, B. M. *Rev. Mod. Phys.* **1981**, *53*, 769.
(30) Lin, S.-L.; Stern, E. A.; Kalb, A. J.; Zhang, Y. *Biochemistry* **1991**, *30*, 2323.
(31) Stern, E. A.; Livings, P.; Zhang, Z. *Phys. Rev. B* **1991**, *43*, 8850.
(32) Joyner, R. W.; Martin, K. J.; Meehan, P. *J. Phys. C*: *Solid State Phys.* **1987**, *20*, 4005.
(33) Riggs-Gelasco, P. J.; Mei, R.; Yocum, C. F.; Penner-Hann, J. E. *J. Am. Chem. Soc.* **1996**, *118*, 2387.
(34) Clark-Baldwin, K.; Tierney, D. L.; Govindaswamy, N.; Gruff, E. S.; Kim, C.; Berg, J.; Koch, S. A.; Penner-Hann, J. E. *J. Am. Chem. Soc.* **1998**, *120*, 8401.
(35) Wong, J.; Lytle, F. W.; Messmer, R. P.; Maylotte, D. H. *Phys. Rev. B* **1984**, *30*, 5596.
(36) Nabavi, M.; Taulelle, F.; Sanchez, C.; Verdaguer, M. *J. Phys. Chem. Solids* **1990**, *51*, 1375.
(37) Bair, R. A.; Goddard, W. A. I. *Phys. Rev. B* **1980**, *22*, 2767.
(38) Yoshida, S.; Tanaka, T.; Hanada, T.; Hiraiwa, T.; Kanai, H.; Funabiki, T. *Catal. Lett.* **1992**, *12*, 277.
(39) Ressler, T.; Wong, J.; Roos, J. *J. Synchrotron Radiation* **1999**, *6*, 656.
(40) Karakida, K.-I.; Kozo, K. *Inorg. Chim. Acta* **1975**, *13*, 113.
(41) Fujikawa, T.; Rehr, J. J.; Wada, Y.; Nagamatsu, S. *J. Synchrotron Radiation* **1999**, *6*, 317.
(42) Vaarkamp, M. *Catal. Today* **1998**, *39*, 271.
(43) Palmer, K. J. *J. Am. Chem. Soc.* **1938**, *60*, 2360.
(44) Galy, J.; Enjalbert, R.; Jugie, G.; Strahle, J. *J. Solid State Chem.* **1983**, *47*, 143.
(45) Huang, H.; DeKock, C. W. *Inorg. Chem.* **1993**, *32*, 2287.
(46) Gosink, H.-J.; Roesky, H. W.; Noltemeyer, M.; Schmidt, H.-G.; Freier-Erdmegger, C.; Sheldriek, G. M. *Chem. Ber.* **1993**, *126*, 279.
(47) Rulkens, R.; Male, J. L.; Terry, K. W.; Olthof, B.; Khodakov, A.; Bell, A., T.; Iglesia, E.; Tilley, T. D. *Chem. Mater.* **1999**, *11*, 2966.
(48) Feher, F. J.; Walzer, J. F.; Blanski, R. L. *J. Am. Chem. Soc.* **1991**, *113*, 3618.
(49) Motevalli, M.; Shah, D.; Sha, S. A. A.; Sullivan, A. C. *Organometallics* **1994**, *13*, 4109.
(50) van der Gaauw, A.; Wilkin, O. W.; Young, N. A. *J. Chem. Soc., Dalton Trans.* **1999**, 2405.
(51) Hanawalt, J. D. *Z. Phys.* **1931**, *70*, 293.
(52) Vaarkamp, M.; Dring, I.; Oldman, R. J.; Stern, E. A.; Koningsberger, D. C. *Phys. Rev. B* **1994**, *50*, 7872.
(53) An equally good fit could be obtained by postulating a two-site model, in which half of the vanadium sites have two short V−Cl distances and half have two long V−Cl distances. While mathematically indistinguishable from the model in which all sites have one short and one long V−Cl distance, we believe the two-site model is chemically unreasonable, considering that all sites appear to have the same V═O and V−OSi distances.
(54) Teo, B.-K.; Lee, P. A. *J. Am. Chem. Soc.* **1979**, *101*, 2815.
(55) Riggs-Gelasco, P. J.; Stemmler, T. L.; Penner-Hann, J. E. *Coord. Chem. Rev.* **1995**, *144*, 245.
(56) Rohlf, F. J.; Sokal, R. R. *Statistical Tables*, 2nd ed.; Freeman: San Francisco, CA, 1981.
(57) Priebsch, W.; Rehder, D. *Inorg. Chem.* **1990**, *20*, 3013.
(58) Branch, C. S.; Bott, S. G.; Barron, A. R. *J. Organomet. Chem.* **2003**, *666*, 23.
(59) Pinkus, A. G.; Ku, A. T. Y. *J. Org. Chem.* **1966**, *31*, 1094.
(60) Prokof'ev, A. I.; Prokof'eva, T. I.; Belostotskaya, I. S.; Bubnov, N. N.; Solodovnikov, S. P.; Ershov, V. V.; Kabachnik, M. I. *Tetrahedron* **1979**, *35*, 2471.
(61) Deiters, J. A.; Holmes, R. R.; Holmes, J. M. *J. Am. Chem. Soc.* **1988**, *110*, 7672.
(62) Negrebetsky, V. V.; Shipov, A. G.; Kramarova, E. P.; Negrebetsky, V. V.; Baukov, Y. I. *J. Organomet. Chem.* **1997**, *530*, 1.
(63) Macharashvili, A. A.; Shklover, V. E.; Struchkov, Y. T.; Gostevskii, B. A.; Kalikhman, I. D.; Bannikova, O. B.; Voronkov, M. G.; Pestunovich, V. A. *J. Organomet. Chem.* **1988**, *356*, 23.
(64) Lang, S. A.; Morrow, B. A. *J. Phys. Chem.* **1994**, *98*, 13314.
(65) Molapo, D. T. Ph.D. Thesis, University of Ottawa, 1998.
(66) Plyuto, Y. V.; Gomenyuk, A. A.; Babich, I. V.; Chuiko, A. A. *Kolloid. Zh.* **1993**, *55*, 85.